

# Encoding Tactile Stimuli for Braille Recognition with Organoids

Tianyi Liu<sup>1</sup> Hemma Philamore<sup>1</sup> Benjamin Ward-Cherrier<sup>1,\*</sup>

<sup>1</sup>School of Engineering Mathematics and Technology, University of Bristol, Bristol, United Kingdom

Corresponding author: [b.ward-cherrier@bristol.ac.uk](mailto:b.ward-cherrier@bristol.ac.uk)

## Abstract

This study proposes a transferable encoding strategy that maps tactile sensor data to electrical stimulation patterns, enabling neural organoids to perform an open-loop artificial tactile Braille classification task. Human forebrain organoids cultured on a low-density microelectrode array (MEA) are systematically stimulated to characterize the relationship between electrical stimulation parameters (number of pulse, phase amplitude, phase duration, and trigger delay) and organoid responses, measured as spike activity and spatial displacement of the center of activity. Implemented on event-based tactile inputs recorded from the Evetac sensor, our system achieved an average Braille letter classification accuracy of 61% with a single organoid, which increased significantly to 83% when responses from a three-organoid ensemble were combined. Additionally, the multi-organoid configuration demonstrated enhanced robustness against various types of artificially introduced noise. This research demonstrates the potential of organoids as low-power, adaptive bio-hybrid computational elements and provides a foundational encoding framework for future scalable bio-hybrid computing architectures.

## Keywords

neural organoids; organoid intelligence; bio-hybrid computing; multiparameter encoding; open-loop tactile classification; Braille classification; low-density MEA

## 1 Introduction

Silicon-based neuromorphic processors achieve notable energy savings when compared to traditional Von Neumann computing systems. Systems such as IBM's TrueNorth [1] or Intel's Loihi [2] operate in the milliwatt range by fusing memory and computation and

firing only when events occur. However, when engineers scale these chips toward cortex-level complexity, projected power climbs into the kilowatt-megawatt bracket, whereas the human brain performs comparable computation on roughly 20 watts [3].

Wet neuromorphic computing bypasses the energy limit on these silicon systems by using brain organoids grown on multielectrode arrays. These living networks have 3-D architecture and genuine synapses that reorganize and learn while consuming orders of magnitude less energy [4]. Such capabilities emerge only when three layers operate as one stack: wetware (the organoid), hardware (microfluidic culture, MEAs, optical, and bio-CMOS sensors that keep the tissue alive and observable) and software (millisecond closed-loop algorithms that read, stimulate, and adapt the network). When these layers are co-designed, organoids shift from spontaneous activity to purposeful information processing [5].

While some research primarily focuses on exploring internal neural dynamics and structure-function relationships within organoid networks, such as drug-induced synaptic modulation [6], critical-state sensory conditioning [7], and spontaneous functional network formation [8], a growing body of work treats neural organoids as computing elements within artificial intelligence frameworks, a field termed Organoid Intelligence (OI). OI leverages the intrinsic plasticity and extremely low power consumption of brain organoids, offering significant potential for creating energy-efficient computing platforms, particularly in robotics and autonomous systems.

Previous studies have demonstrated the computational capabilities of neural organoids. Direction-selective ganglion-cell ensembles not only classified the direction of a moving bright bar but also exploited stimulus-dependent noise correlations to sharpen that estimate [9]. Cortical organoids have acted as “living reservoir” computers that steadily improve at decoding Japanese vowels and chaotic time-series after characterization of their nonlinear dynamics [10]. In the DishBrain Pong paradigm, closed-loop interaction enabled the organoid to steadily improve its performance in the virtual game, indicating that the network had learned the task objective. Cultured neurons shaped into a two-input/one-output pathway on a micro-electrode chip behave as a living logic gate, reliably delivering NAND or OR outputs and demonstrating that basic digital operations can run on biological tissue [11]. George et al. achieved BNN-ANN closed-loop control by bidirectionally linking a neonatal rat spinal CPG slice with an FPGA-based spiking ANN, restoring rhythmic bursts lost in isolation [12]. Ades et al. built a closed-loop biohybrid system in which mouse cortical neurons cultured on a multielectrode array drive a Shadow robotic hand with BioTac sensors [13]. These findings substantiate organoids as feasible substrates for bio-hybrid intelligence, capable of learning, classification, and control in real-world robotic scenarios.

Fully realizing this potential in robotic applications requires effective communication among artificial sensory devices, organoid networks, and external processing-and-actuation

systems. This communication critically relies on suitable encoding and decoding methods. Encoding refers to transforming external sensory data or control signals into stimulation patterns that neural organoids can interpret, typically through electrical, optical, or chemical stimuli. Decoding involves translating the organoid responses into signals that external computational systems can process and interpret. Developing an efficient and generalizable encoding-decoding framework is thus a prerequisite for enabling reliable interactions between robotic sensory systems and neural organoid computing platforms. Despite the variation in organoid architectures and computational roles, multielectrode arrays (MEAs) have become the principal interface for stimulating and recording neural activity. High density MEAs have been successfully employed for closed-loop learning in planar cultures [14] and reservoir computing in organoids [10], however, the cost and availability of such hardware remain limiting [15]. Lower density layouts therefore continue to see extensive use, such as an implementation that positions each human forebrain spheroid above eight stainless-steel electrodes in an air-liquid-interface array and delivers remote recordings through the Neuroplatform [16]. Using this same setup, we demonstrate that organoid intelligence can be elicited and quantified with a low-density MEA.

Prior studies in OI and biohybrid platforms explore strategies that encode stimuli and decode neural responses across varied tasks and organoid preparations. Encoding implementations vary with task demands. Franke et al. employ natural stimuli, sweeping a bright bar across an ex-vivo retina allowing each ganglion cell to convert motion into its innate spike-count tuning, but limiting direct control over stimulus features [9]. Rate-place coding across eight electrodes conveyed ball position to DishBrain cultures, enabling intuitive spatial representations suitable for closed-loop motor learning [14]. Brainware experiments use flexible spatiotemporal encodings tailored specifically to the input type: acoustic features are mapped to electrode location and stimulation amplitude, while scalar time-series are represented as amplitude-scaled pulses delivered at fixed intervals, balancing complexity and adaptability for distinct temporal inputs [10]. The Shadow-Hand system encodes fingertip forces into slowly- and rapidly-adapting spike trains, using timing-only differences to deliver rapid change cues and continuous pressure feedback with a lightweight real-time Izhikevich model [13]. Address-event representation (AER) streams on the GAIA array encode space in the electrode address and time in the timing of each event, thus enabling seamless integration with neuromorphic hardware [17]. Binary values have been represented in hippocampal micro-networks by toggling pulse amplitude or rate on two input lines, but was limited in representing richer analog or multidimensional signals [11]. Decoding usually relies on straightforward spike-based statistics, most often the per-electrode spike count accumulated within a brief post-stimulus window. Alternative metrics such as time-to-first-spike and mean inter-spike interval are also employed [11]. Across their diverse aims, these studies consistently rely on application-specific encoding strategies.

In this work, we propose a general-purpose encoding strategy that is applied to tactile sensory inputs for neural organoid processing, that preserves spatial, temporal and intensity information yet remains compatible with low-density MEAs. Using an event-driven tactile sensor to capture Braille stimuli, we map sensory data into multi-channel electrical stimulation patterns. We demonstrate the feasibility and effectiveness of our method through a tactile Braille letter-classification task. On the remotely accessible FinalSpark Neuroplatform [16], tactile information from a neuromorphic sensor is delivered to human cortical organoids cultured on eight-electrode MEAs, and the decoded organoid activity is subsequently classified with a support vector machine (SVM) [18]. Our experiments show that neural organoids can robustly classify tactile patterns, and that employing multiple organoids in parallel significantly improves classification accuracy and robustness, highlighting the promise of scalable biohybrid computing architectures. Our main contributions in this work are:

- We established a quantitative stimulus-response profile that relates stimulation parameters to organoid spike magnitude, timing and spatial distribution.
- We present a spatio-temporal-intensity encoding that converts event-based tactile data into current-controlled electrical stimulation for organoids on low-density MEAs.
- We demonstrate Braille character classification with organoids reaching 83% accuracy and noise resilience with a three-organoid ensemble.

## 2 Materials and Methods

### 2.1 Organoid and Recording Platform

All our experiments were conducted using FinalSpark’s NeuroPlatform [16], providing access to organoids over a cloud-based system, as shown in Figure 1. In this setup, forebrain organoids are cultured to approximately 500  $\mu\text{m}$  in diameter [19] and contain mature neurons, astrocytes, and oligodendrocytes displaying robust network activity. Maintained under continuous perfusion, they can remain electrophysiologically active for up to approximately 100 days under favourable conditions [16].

The platform consists of a remotely accessible electrophysiology system integrating four custom air-liquid interface MEAs, each accommodating four organoids with eight electrodes per organoid for a total of 32 channels per MEA. Voltage signals are acquired via Intan RHS headstages sampling at 30 kHz with 16-bit resolution. All hardware functions are accessible through a Python API and Jupyter notebook interface, with data continuously archived in an InfluxDB time-series database which can be used for downstream analysis. In this study, the Neuroplatform was accessed remotely for stimulation and recording,

whereas tactile sensing and data preprocessing were performed locally before stimulation was executed.

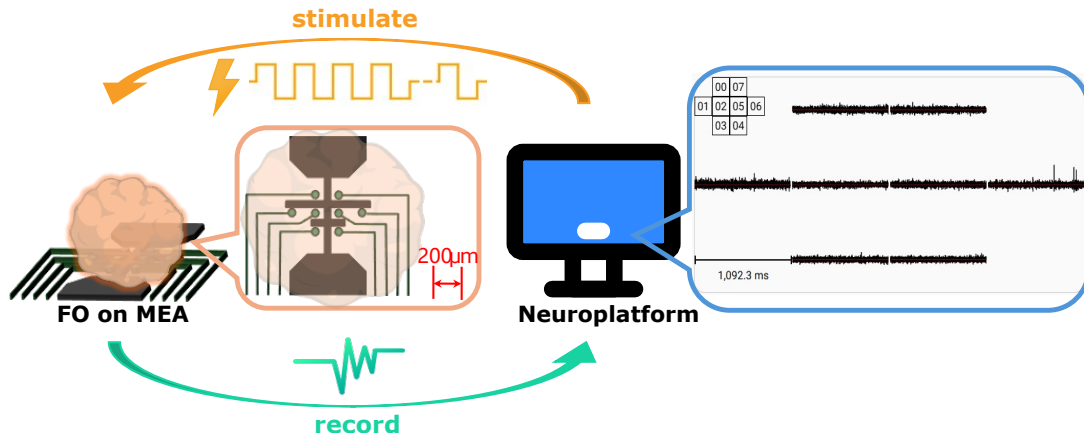


Figure 1: Interaction between a forebrain organoid (FO) cultured on a multi-electrode array (MEA) and the Neuroplatform. The 8 recording electrodes are arranged with  $200\ \mu\text{m}$  centre-to-centre spacing, providing a distributed interface across the organoid. Neural activity is recorded from the FO and electrical stimulation is delivered via a remotely accessible software interface.

## 2.2 The Impact of Electrode Stimulation Parameters on Organoid Responses

Across the three experiments, we tested organoid responses to stimulation parameters representing the stimulus’s temporal, spatial, and intensity dimensions, laying the groundwork for an encoding strategy that converts tactile-sensor outputs into electrical patterns.

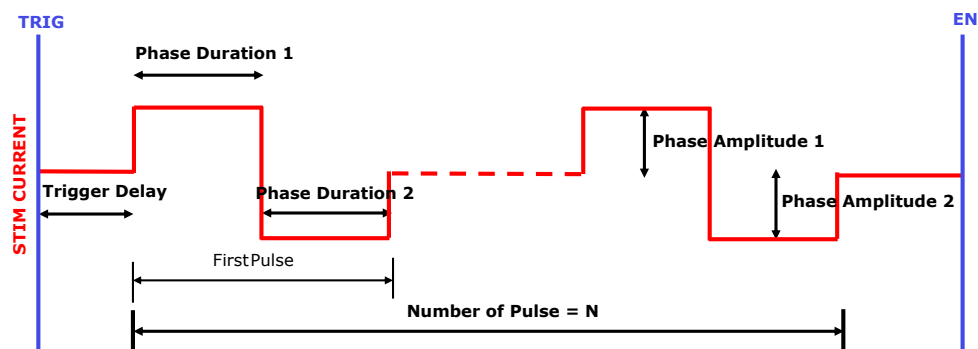


Figure 2: Illustration of adjustable parameters in the Neuroplatform.

As shown in Figure 2, electrical stimulation on the Neuroplatform is parameterized through several key variables [16]. The “shape” of the current waveform may be biphasic, biphasic with an interphase delay, or triphasic. A biphasic waveform consists of a positive phase followed by a negative phase, each specified by an amplitude and a duration. A triphasic waveform consists of three phases with alternating polarity. Each phase is

specified by an amplitude and a duration: Amplitude 1 and Duration 1 for the positive phase, Amplitude 2 and Duration 2 for the negative phase. The polarity of the waveform can be inverted to begin with either a negative or a positive phase. Stimulation can be triggered as a single pulse, as a sequence defined in a trigger table, and can be directed to any subset of the 32 electrodes. The trigger delay parameter controls the onset timing of the first pulse, while the number of pulses parameter specifies how many pulses are delivered in each sequence. Charge balanced biphasic stimulation is widely used because its primary objective is to keep the electrode potential within a safe range, thereby reducing irreversible electrochemical reactions that can degrade the electrode or damage tissue [20]. In all experiments, we chose a positive first and negative second biphasic voltage waveform because it statistically produces the lowest neural activation thresholds while safeguarding both the electrode and surrounding cells over the long term [21]. To improve the lifetime of both the organoid and the electrodes, we set Phase Amplitude 1 = Phase Amplitude 2 and Phase Duration 1 = Phase Duration 2. We used the Neuroplatform default interphase delay of 0  $\mu\text{s}$  between the two phases, and default pulse train period of 10000  $\mu\text{s}$  for pulse trains.

### 2.2.1 Organoid Responses Under Different Stimulation Parameters

In this experiment, we map the effective stimulation range by testing whether electrical input produces significant departures from spontaneous activity and whether different parameter values elicit statistically separable response profiles. Values that meet both criteria become candidate parameters for the encoding scheme. Finally, we assess whether parameter–response relationships are consistent across electrodes to determine if encoding must be tailored for each electrode.

The experiment involves stimulating each electrode within the same organoid respectively, recording data from all electrodes and averaging across them to observe the overall effect of stimulation parameters on the organoid output. Stimuli are delivered with a 2 s inter-stimulus interval to allow sufficient recovery and avoid temporal summation. Here, one stimulus refers to a single trial consisting of a pulse train with 1 to 10 pulses, the interpulse timing within the train is set by the platform default 10000  $\mu\text{s}$  pulse train period. We record the number of spikes generated across all channels within a 200 ms window following stimulation and compute the mean over 10 trials. We test various numbers of pulses (0 to 10), phase amplitudes (0 to 20  $\mu\text{A}$ ), phase durations (0 to 200  $\mu\text{s}$ ), and trigger delays (0 to 4000  $\mu\text{s}$ ). A parameter value of 0 indicates spontaneous activity recorded under the unstimulated (spontaneous) condition. During each individual sweep, the remaining parameters are kept at their default values: a single pulse, 4  $\mu\text{A}$  phase amplitude, and a 100  $\mu\text{s}$  phase duration. These base parameters were selected to provide a simple and interpretable reference condition for one factor sweeps. We used a single pulse

as the minimal stimulation form, minimizing temporal summation effects and prolonged network activation. We set the phase amplitude to  $4 \mu\text{A}$  because lower amplitudes were typically subthreshold in our recordings, while higher values risked driving near-saturated responses, and chose a  $100 \mu\text{s}$  phase duration as a mid-range value within the sweep to avoid boundary effects.

### 2.2.2 Temporal Dynamics of Organoid Responses

We then investigate how long the effect of a single stimulation persists, to determine the appropriate time window for each sample in the Braille experiment. All channels of the same organoid are simultaneously stimulated with identical parameters; the average spike count across all channels is recorded over a 600 ms window around the stimulus.

Stimulation parameters explored in this experiment are as follows: numbers of pulses (1 - 10 pulses), amplitude (2 - 20  $\mu\text{A}$ ), and phase duration (25 - 200  $\mu\text{s}$ ). We sweep one parameter at a time through its range while keeping the other two fixed at their default values of a single pulse,  $4 \mu\text{A}$ , and  $100 \mu\text{s}$ . Each parameter condition is repeated 10 times with a 2 s inter-stimulus interval to allow recovery. We record spike counts from 100 ms before stimulation to 500 ms after stimulation across all channels and average over 10 trials.

### 2.2.3 Spatial Dynamics of Organoid Responses

We adopted the method of Jordan et al. [16] to estimate the spatial center of activity (CA) after each stimulus, thereby quantifying shifts in overall network firing. The CA is the weighted centroid of spikes recorded on the organoid’s eight electrodes. For a 500 ms analysis window, with spike count  $F_k$  and normalized coordinates  $(X_k, Y_k)$  at electrode  $k$ , the CA vector  $\mathbf{C}$  is:

$$\mathbf{C} = \frac{\sum_{k=1}^8 F_k \cdot (X_k, Y_k)}{\sum_{k=1}^8 F_k} \quad (1)$$

We first recorded the CA during spontaneous activity to establish a baseline. For each stimulation condition, we recorded spike data from all electrodes within a 500 ms post-stimulation window. We systematically tested and recorded the organoid responses by stimulating each electrode with varying numbers of pulses (2, 4, 6, 8, and 10), phase amplitudes (4, 8, 12, 16, and 20  $\mu\text{A}$ ), and phase durations (50, 100, 150, 200, and 250  $\mu\text{s}$ ). The default stimulation parameters are set to a pulse count of 5, a phase amplitude of 10  $\mu\text{A}$ , and a phase duration of 150  $\mu\text{s}$ , corresponding to the midpoints of their respective parameter ranges. This keeps the reference condition away from both near-threshold and near-saturation regimes, so that changes induced by the swept parameter are more readily observable and less affected by boundary effects. Each condition is repeated 100 times

with a 500 ms inter-stimulus interval.

The CA displacement relative to baseline shows how population firing migrates within the organoid. By analysing these displacements we test whether assigning different regions of the tactile sensor to distinct electrodes preserves spatial information and whether varying stimulus magnitudes elicits distinguishable network responses.

## 2.3 Applying Organoid Intelligence to Braille Classification

Earlier stimulation tests showed that variations in pulse amplitude, width and count elicit distinct firing patterns in the organoid (see Section 3.1). Building on these results, we design an encoding pipeline that converts event based tactile signals into electrical stimulation patterns and applies straightforward machine learning classifiers to the resulting organoid activity.

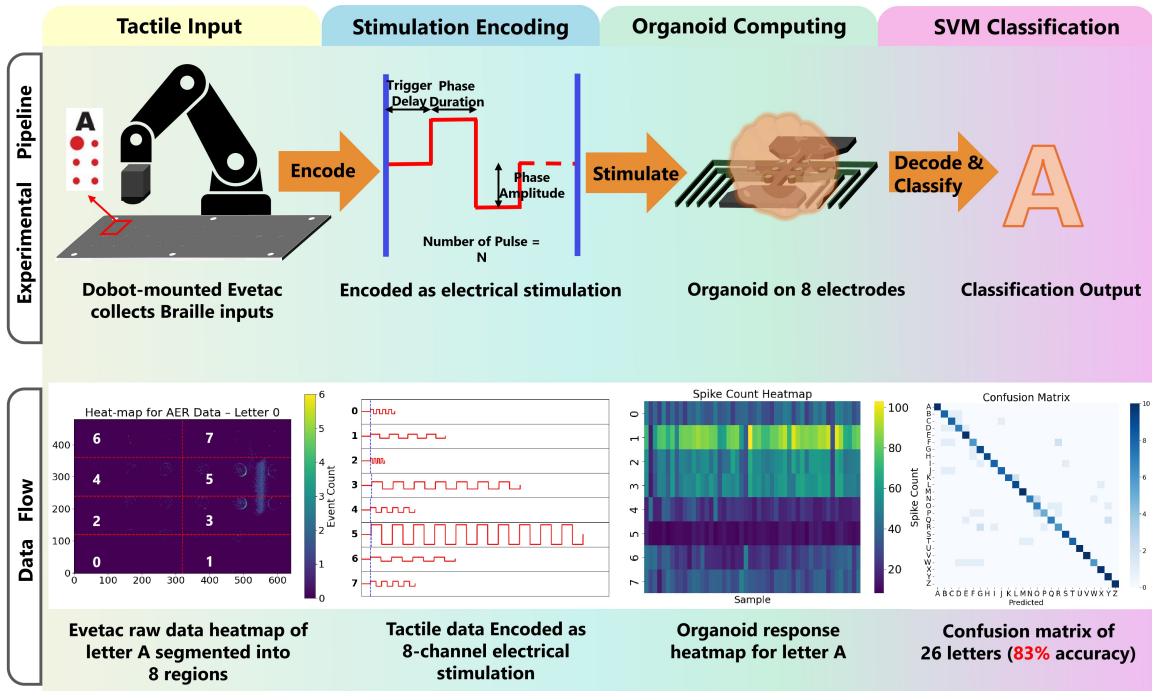


Figure 3: Experimental procedure for collecting Braille using a tactile sensor, encoding it into electrical stimulation, delivering it to organoids, and classifying 26 Braille letters based on organoid outputs. The first row outlines the experimental steps, and the second row shows the type of data associated with each step.

### 2.3.1 Experimental Setup and Data Collection

An Evetac optical tactile sensor [22] was mounted on the end effector of a four-axis Dobot MG400 robotic arm [23]. The sensor contains a soft silicone gel embossed with a regular grid of black markers, an internal LED ring for uniform illumination and a DVXplorer Mini event camera housed in a 3d-printed enclosure. Gel indentation displaces

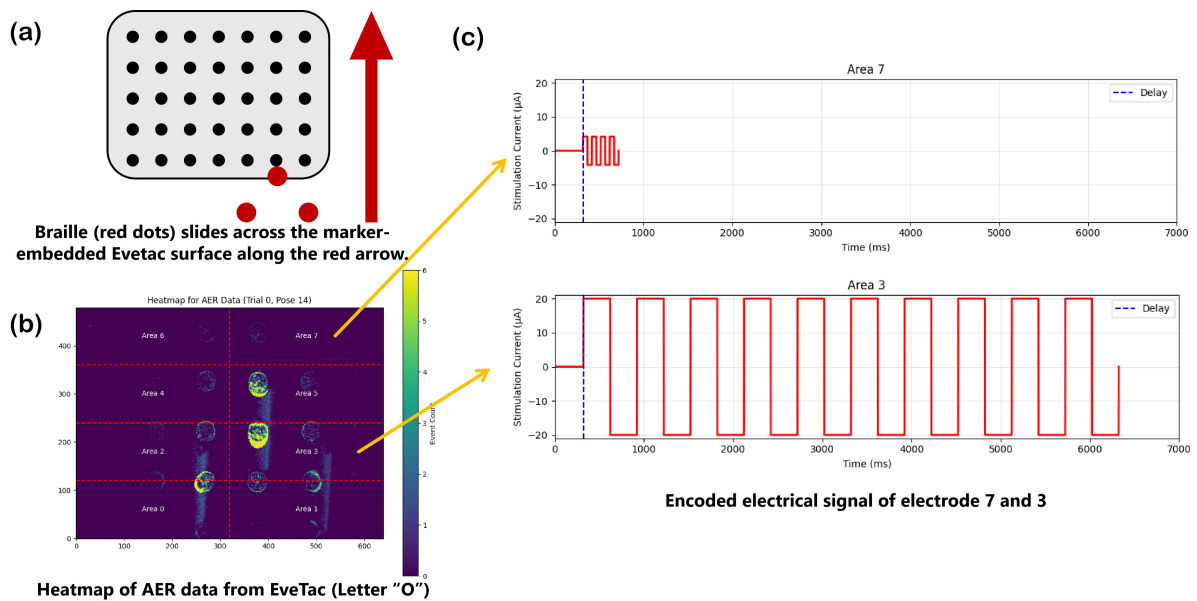
the markers, the accompanying motion and shadow pattern modulate local brightness, generating asynchronous pixel events that the camera exports every millisecond. Each event carries its pixel address, polarity and a microsecond time stamp and is streamed in Address-Event Representation (AER) format [24]. Evetac resolves vibrations up to 498 Hz and captures shear forces and incipient slip [22], making it suitable for fast Braille exploration. Tactile stimuli are delivered with a 3D-printed Braille board that held the 26 English letters arranged in three rows of nine, nine and eight characters. The plate measures 23×14 cm, and adjacent letters are separated by 2.2 cm.

The overall pipeline is as displayed in Figure 3. First, Braille characters are sampled using the Evetac sensor [22]: for each of the 26 Braille letters, the Evetac is lowered to a given depth (0, 0.1, 0.2, 0.3, 0.4 mm) and slid horizontally across the Braille character for 10 trials, yielding 1300 recordings in total. Depth 0 denotes the initial shallow indentation upon contact. Next, we encode this AER data into stimulation patterns for the organoid’s 8 electrodes (as detailed in section 2.3.2) Then stimulation patterns for the different Braille characters are delivered to the organoid and the organoid’s response is read out as an 8-dimensional response vector of spike counts across the organoid’s eight channels. Finally, appropriate classifiers are applied to distinguish among the 26 Braille letters based on organoid responses. We test KNN [25], SVM [18], and random forest [26] classifiers, ultimately selecting SVM as the best-performing option.

### 2.3.2 Electrical Encoding of Tactile Event Features

We partition the Evetac output into eight spatial regions that correspond to the organoid’s eight channels and introduce an encoding that embeds spatiotemporal intensity information to convert tactile events into electrical stimulation. From the AER data [27], four key features are extracted for each region:

- **Event count:** the total number of events in the region, representing overall tactile intensity. Here, an “event” refers to a single AER pixel event with an address, polarity, and timestamp. The event count for a region is computed as the total number of raw AER events whose pixel addresses fall within that region, summed over the full 2000 ms tactile recording.
- **Event duration:** the time difference between the first and last events, representing the duration of tactile contact.
- **Time of peak activity:** the midpoint time of the 100 ms window with the highest event count, indicating when the Braille character reaches that region (original data length was 2000 ms).
- **Event deviation:** the deviation of event counts across 100 ms windows, representing temporal variation in tactile intensity.



Area → Electrode	Event count → Number of pulse	Event duration → Phase duration	Time of peak activity → Trigger delay	Event deviation → Phase amplitude
7	277	4	366 ms	50
3	13,389	10	399 ms	300
			16,050 ms	32,100 us
			16,150 ms	32,300 us
			12	4.18
			570	20

Figure 4: Illustration of the encoding strategy. (a) Schematic showing the Braille character (red dots) sliding across the marker-embedded Evetac surface along the direction of the red arrow. (b) The output of the neuromorphic tactile sensor in the form of a heatmap, where the colorbar indicates the number of events and brighter colors represent higher event counts. (c) The corresponding electrical stimulation encoding for different regions of the original data. The table below shows an example of the encoding results from sensor outputs in Area 3 and 7 to electrical stimulation parameters.

We select four key stimulation parameters for the organoids: number of pulses, phase duration, trigger delay, and phase amplitude, and all electrodes use the same encoding range. These parameters control the timing and strength of the stimulation delivered to the organoid. For each AER recording, each extracted feature is linearly mapped to its corresponding stimulation parameter:

- **Number of pulses:** controls the number of pulses in each spike train to convey tactile strength; mapped to 4–10.
- **Phase duration:** controls the duration of each pulse to convey tactile duration; mapped to 50–300  $\mu\text{s}$ .
- **Trigger delay:** controls the time to start the stimulation to convey when the tactile event begins; mapped to 0–4000  $\mu\text{s}$ .
- **Phase amplitude:** controls pulse strength to convey temporal variation of tactile intensity; mapped to 4–20  $\mu\text{A}$ .

We set a 1 s inter-sample interval to allow recovery, and use spikes evoked within 500 ms post-stimulation as organoid output, as shown in Figure 4 for a sample encoding of the letter O.

### 2.3.3 Organoid Decoding and Classification Under Noisy Conditions

We decode the spike patterns that emerge from the organoid’s own network dynamics after each stimulus. For each stimulus, we count the spikes detected on each electrode during the 500 ms interval following stimulation. Since each organoid is connected to 8 electrodes, the resulting spike activity forms an 8-dimensional feature vector, which is then used by a support vector machine classifier to identify the Braille character. To study the effect of scale, we repeat the experiment with 3 organoids in parallel. The same 8-region encoding drives each organoid, we record all 8 channels from every organoid, and we concatenate them into a 24-dimensional feature vector before classification.

To assess robustness, we introduce artificial disturbances to the spike-count features while keeping the original tactile dataset unchanged. The tactile data are collected at 5 different depths, which already introduces inherent variability, the additional disturbances are applied on top of this. Specifically, we randomly select 4 channels in the feature vector and modify only those values. We apply 4 disturbance models: additive Gaussian noise with a standard deviation equal to 40% of the channel standard deviation, additive uniform noise within the same range, data loss where 40% of the selected entries are set to zero, and outliers where 40% of the selected entries are multiplied by 3. We then report support-vector machine accuracy under each model to quantify how single and triple organoid decoders tolerate channel interference. These models are not intended

to cover every realistic sensor artifact, but to provide a basic stress test of whether the performance benefit of using multiple organoids remains under several common types of channel corruption.

## 3 Results

### 3.1 The Impact of Electrode Stimulation Parameters on Organoid Responses

In this section, we examine how individual electrode stimulation parameters affect organoid responses. We quantify effects in three aspects: spike count, temporal dynamics, and spatial dynamics. Spike counts are analyzed through controlled parameter sweeps with trend visualizations to reveal overall patterns. Temporal dynamics are characterized from response profiles within a fixed readout window after stimulation. Spatial dynamics are assessed using a set of three metrics to evaluate displacement and the clustering and dispersion of organoid responses. The combined evidence guides the selection and mapping ranges of stimulation parameters for converting tactile inputs into electrical stimuli for the organoid system.

#### 3.1.1 Organoid Responses Under Different Stimulation Parameters

This experiment tests how spike output varies when one stimulation parameter changes at a time, guiding the choice of safe and informative encoding ranges. Stimulating each electrode in turn and recording from all eight channels reveals clear trends (Figure 5). Spike count increases almost linearly as the number of pulses rises and shows a threshold for phase amplitude: values below  $4 \mu\text{A}$  rarely evoke spikes, whereas higher amplitudes produce steadily larger responses. In this one-factor sweep, phase duration does not produce a consistent monotonic trend in spike count across the tested conditions, and trigger delay has no observable effect on spike count. Under the no stimulation condition, the spike count measured within the same 200 ms post-trigger window is often close to zero. This reflects the combination of sparse spontaneous firing and the short counting window, rather than an absence of spontaneous activity.

Taken together, the observed response trends motivate the following encoding choices. The similarity across electrodes supports adopting a common encoding range for all channels. Phase amplitude is set above the activation threshold while remaining within safe limits. Pulse count is chosen from the region where spike output increases approximately linearly, enabling graded intensity. Although phase duration and trigger delay do not show a clear correlation with spike number, varying them produces distinct temporal patterns, so both are retained to encode timing information.

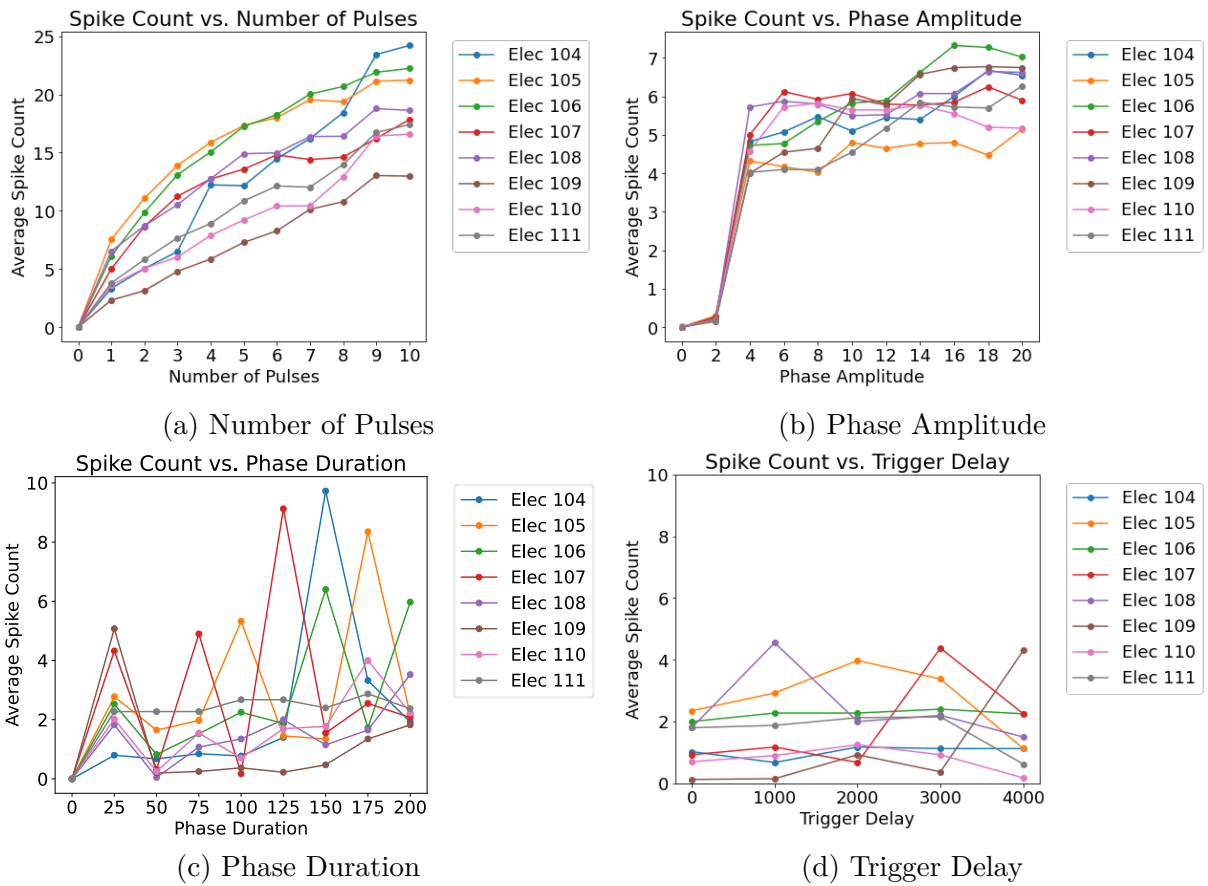


Figure 5: Relationship between stimulation parameter values and the total spike count across all channels of the organoid. The x-axis represents the parameter value, and the y-axis indicates the average spike count across all channels. Lines represent the index of the stimulated electrode.

### 3.1.2 Temporal Dynamics of Organoid Responses

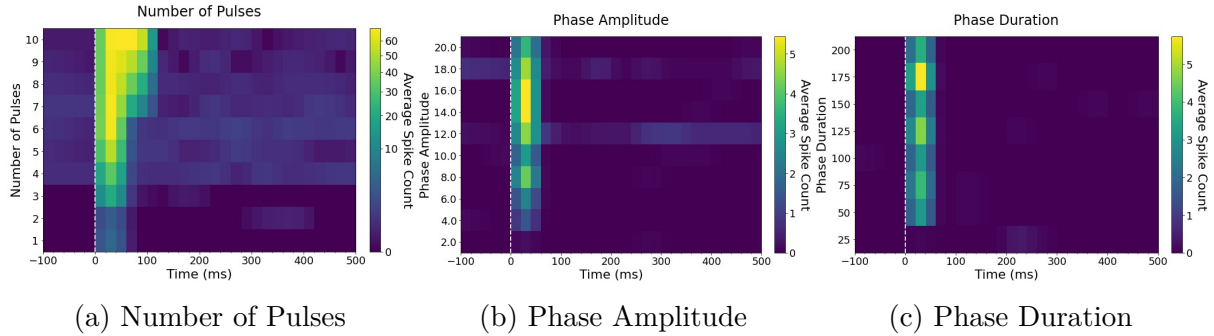


Figure 6: Relationship between stimulation parameter value and duration of the stimulation effect. (a) Number of Pulses. (b) Phase Amplitude. (c) Phase Duration. In each heatmap, the x-axis displays time from 100 ms before to 500 ms after stimulation, while the y-axis represents the varying parameter values. The color intensity indicates the average spike count of the organoid, with brighter colors representing higher activity levels. The vertical dashed line at  $t=0$  indicates the stimulation onset.

This experiment measures how long each stimulus influences network firing. In this experiment, we apply simultaneous stimulation across all electrodes with varying parameters and partition the recording into 20 ms windows, as shown in Figure 6. The dashed line marks stimulation onset.

When a single pulse is delivered, most responses return to the pre-stimulation activity level within 60 ms. Figure 6a shows that increasing the pulse count effectively prolongs the duration of the evoked activity, extending the response to approximately 100 ms at higher pulse counts. Figure 6b again shows that phase amplitudes below  $4 \mu\text{A}$  fail to evoke responses, whereas larger amplitudes do not uniformly increase spike count, they result in distinguishable intensities of activation within the post-stimulation window. Even a  $50 \mu\text{s}$  pulse triggers a clear spike burst (Figure 6c), in line with earlier reports [21]. These findings motivate a 500 ms analysis window for each trial in the Braille experiment. The window captures all evoked spikes yet remains short enough that the sparse spontaneous activity in our organoids rarely appears. The Neuroplatform’s adaptive threshold references each electrode’s baseline level, making sure a majority of spikes detected in this window arise from the stimulus.

### 3.1.3 Spatial Dynamics of Organoid Responses

This experiment assesses how stimulation parameters reshape the spatial pattern of activity across the organoid. Each stimulus value was applied individually to every stimulating electrode; for each electrode-parameter pair we recorded 100 trials, yielding a 100-point activity-centre (CA) cluster. The 100 CA locations from one electrode at one setting form a cluster, points in the same cluster share the same electrode and parameter, whereas

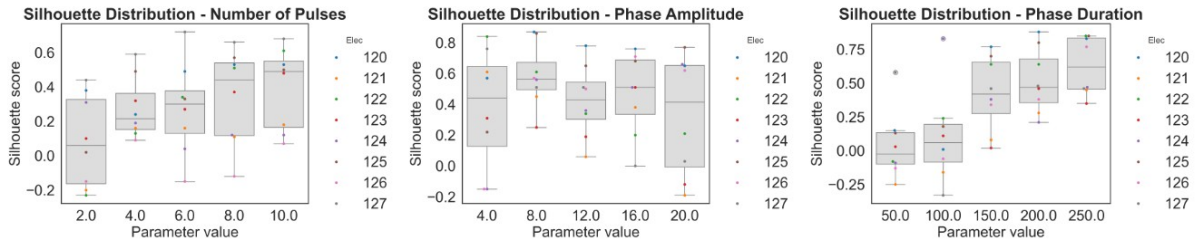
points in different clusters share the parameter but not the electrode. To characterise how a stimulus reshapes these clusters, we computed three quantitative metrics:

- **Silhouette score:** Combines intra-cluster tightness with inter-cluster separation. A higher score indicates a CA cloud that is simultaneously compact and well isolated from those elicited by the other electrodes.
- **Centroid shift from baseline:** Euclidean distance between the stimulated cluster centroid and the spontaneous (no-stimulus) CA centroid. This captures the spatial displacement produced by the stimulus.
- **Global spike count:** Total spikes across the eight recording channels, averaged over the 100 repetitions. This reflects the overall population excitability evoked by the stimulus.

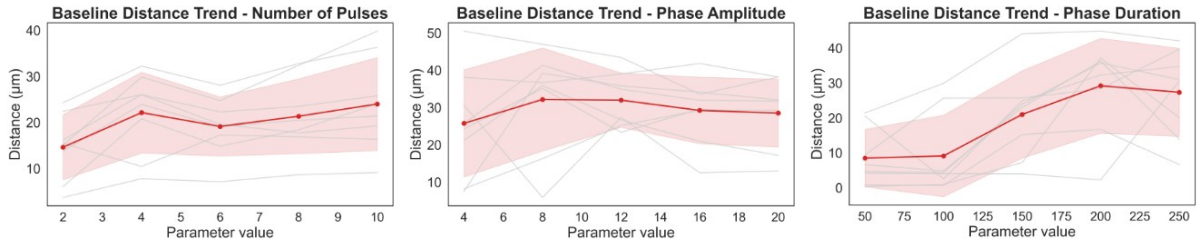
Figure 7 congregates the three quantitative descriptors into aligned panels so that the influence of each stimulus family can be followed across electrodes and then integrated in Figure 7d. In the radar plots each metric is first min-max normalised to 0-1 using the global extrema across all parameters and electrodes, then averaged over electrodes. Sharing the same (min, max) pair places every radius on a common percentile scale, producing unit-free polygons that can be compared directly between parameter values and across protocols.

With pulse count the upward trend is most evident between two and four pulses: the median Silhouette score almost doubles and the CA centroid shifts from 14  $\mu\text{m}$  to roughly 22  $\mu\text{m}$ , beyond 4 pulses the curves flatten and subsequent gains are modest. Therefore, we consider that when the number of pulses is greater than or equal to 4, the organoid tends to produce more stable and more distinguishable outputs. For phase amplitude the three metrics increase gradually: the centroid shift moves from 25  $\mu\text{m}$  at 4  $\mu\text{A}$  to 32  $\mu\text{m}$  at 12  $\mu\text{A}$ , with little change thereafter, and the Silhouette curve shows a similar muted rise before plateauing. By contrast, phase duration yields a more sustained escalation across the entire range tested, raising the Silhouette score from close to 0 to 0.63 and displacing the centroid by almost 30  $\mu\text{m}$  while steadily boosting global spike output.

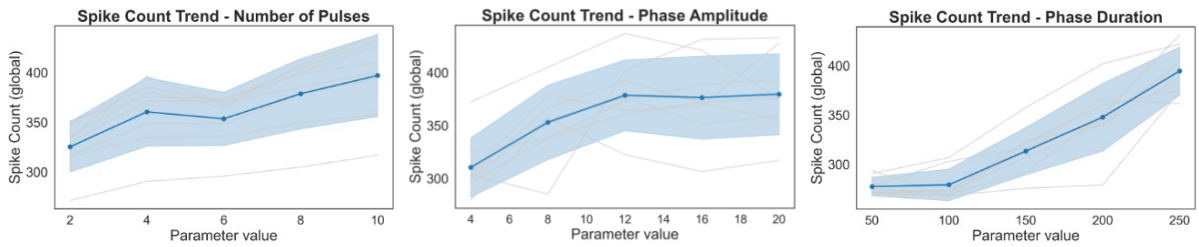
Because pulse counts of four and above give more compact and separable center-of-activity clusters, we restrict the Braille encoding to four to ten pulses, a range that retains efficacy while avoiding overstimulation. Applying identical stimulation to different electrodes shifts the activity center by roughly 20  $\mu\text{m}$  (Figure 7b), showing that routing distinct tactile regions to distinct electrodes can convey spatial information. The shift direction, however, does not track electrode position in a simple one-to-one fashion, and response strength depends on the local network state around each electrode. That is, a region with stronger tactile intensity does not necessarily elicit a stronger response from



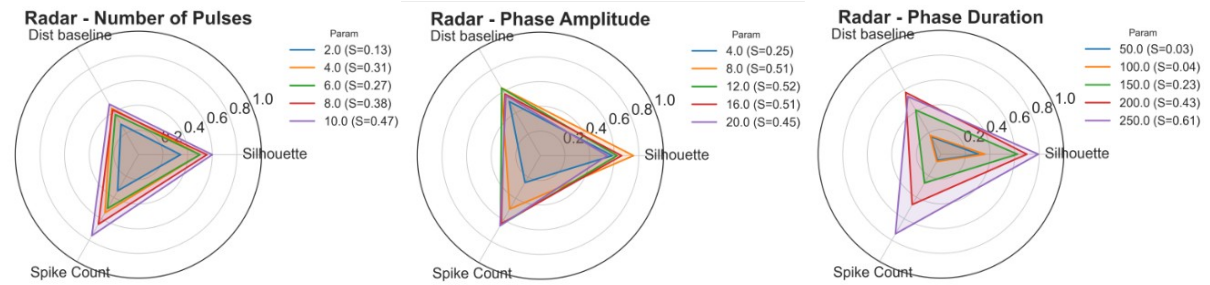
(a) Silhouette Distribution



(b) Baseline-centroid Shift



(c) Global Spike Count



(d) Radar Summaries

Figure 7: From left to right the three columns correspond to Number of Pulses, Phase Amplitude, and Phase Duration. (a) Silhouette Distributions. Box-and-swarm plots show cluster compactness/separation for each stimulating electrode. (b) Baseline-centroid Shift. Grey lines are per-electrode distances from the spontaneous centroid, the red line  $\pm$  band is the array mean  $\pm$  SD. (c) Global Spike Count. Analogous representation for total evoked spikes, with blue mean  $\pm$  SD. (d) Radar Summaries. Three-axis polygons (Silhouette, baseline shift, spike count) condense the metrics for every parameter value, legend lists parameter and polygon area  $S$ .

the corresponding electrode. The organoid therefore imposes its own intrinsic mapping between input location and population response.

### 3.2 Performance of Organoid in Braille Classification

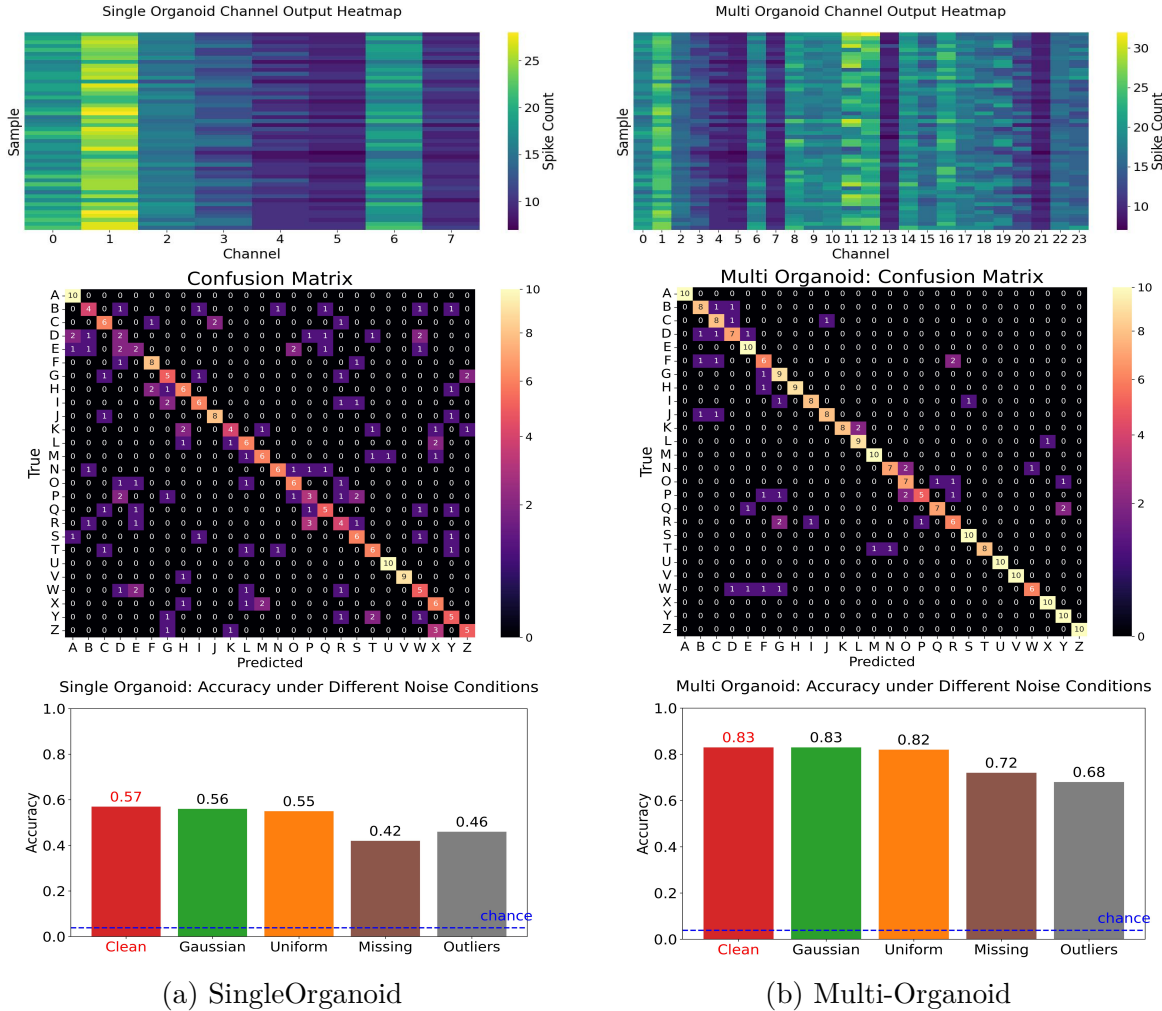


Figure 8: Organoid output, Braille confusion matrix, and robustness to noise. (a) Results from using a single organoid. (b) Results from using three organoids. From top to bottom: a heatmap of organoid output (each row corresponds to one tactile sample, each column to one electrode, with color indicating spike count); a confusion matrix showing classification of decoded organoid responses into 26 Braille letters using an SVM; and classification accuracy under different types of noise, where the red bar indicates performance without added noise. Chance level for 26 letters classification is 3.85%.

As described previously in Section 2.3.2, tactile stimuli from the Evetac sensor are encoded into electrical stimulation patterns based on four parameters: phase amplitude, pulse count, phase duration, and trigger delay. Each tactile input is spatially partitioned into eight regions corresponding to the eight electrodes of the MEA. Organoid responses are decoded by counting spikes from each electrode within a 500 ms readout window. Here,

we assess the effectiveness of this encoding and decoding strategy through the performance of the organoid system in classifying 26 Braille letters.

We use a support vector machine (SVM) classifier with cross-validation on 1300 response vectors for all classification analyses reported in this study. When using only the 8-dimensional output from a single organoid for classification, the accuracy remains stable at approximately 57% (Figure 8a). When conducting experiments with three organoids on the same MEA and using their individual 8-dimensional outputs separately for classification, the accuracies are 59%, 62%, and 67%, respectively. However, when combining the outputs of the three organoids into a 24-dimensional vector, the classification accuracy using SVM reaches 83% (Figure 8b).

As shown in Figure 8, the heatmaps of organoid responses to each sample show that even though different pressing depths are used during data collection, the response patterns of the organoid remain relatively consistent, which indicates that the organoid network exhibits intrinsic robustness to variations in stimulus strength. Comparing the input and output heatmaps further confirms that a stronger indentation in a given sensor region does not always elicit a stronger response from the electrode assigned to that region. The transformation from tactile input to spike output is therefore shaped by local network dynamics rather than by a direct intensity mapping. When noise is introduced again, the single-organoid system’s accuracy decreases by 2.1–26.5% relative to its clean (no-noise) baseline, with ‘missing’ and ‘outliers’ noise causing the largest drops; the three-organoid system’s accuracy decreases by 0.8–18.1% relative to its clean baseline. Here, the reported ranges are taken across the four noise models. These results demonstrate that organoid redundancy enhances resistance to data disturbances.

## 4 Discussion

By systematically characterizing the stimulus-response profile of human forebrain organoids cultured on FinalSpark’s low-density eight-electrode MEA, we developed a transferable spatio-temporal-amplitude encoding strategy that converts spike-based outputs from a neuromorphic sensor into electrical-stimulation patterns that can be processed by the organoid network. Applied to a blind Braille-letter classification benchmark, the encoder demonstrated competitive performance, and multiplexing three organoids in parallel raised accuracy to 83% while markedly improving robustness against Gaussian, uniform, data loss and outlier noise. Collectively, these results show that even sparsely instrumented organoids can support reliable open loop classification when supplied with appropriately structured stimulation input, laying essential groundwork for scalable bio-hybrid computing architectures.

## 4.1 Toward a Transferable Encoding Strategy via Stimulus Parameter Optimization

Increasing the number of pulses is the most direct way to evoke burst-type activity: trains of four or more pulses reliably boost spike counts, especially when combined with higher phase amplitude, which together determine overall stimulus strength. Phase duration is chiefly a temporal variable; it sets the length of each biphasic pulse, defines the integration window for incoming charge, and only secondarily modulates response magnitude. Trigger delay merely schedules when the train begins and does not alter the total charge delivered. Our findings are consistent with the amplitude and pulse-width dependencies reported by Wagenaar et al. [21]; spike output rises steadily with larger amplitudes and longer pulses, displays a clear threshold, and can still be elicited by very brief stimuli. They also align with Li et al. [28], who identified five pulses per train as minimally effective, while our data show that four pulses already provide robust network engagement. Although each electrode on the LD-MEA samples a micro-ensemble of neurons rather than single units, the array still offers enough resolution to expose these parametric trends, confirming that even low-density hardware can capture population-level stimulus–response rules. These four timing-and-strength parameters, combined with electrode location, form the basis of our spatio-temporal-amplitude encoding strategy.

Our proposed encoding strategy is easily adaptable to different tactile sensing tasks and sensor configurations. Spatial resolution can be flexibly adjusted along either spatial dimension depending on task requirements. For instance, tasks like static pressing or shape recognition, where no dominant sliding direction exists and tactile events are uniformly distributed, benefit from a symmetric spatial grid. Conversely, scenarios involving a clear sliding direction, such as Braille reading or texture scanning, are better served by increasing resolution along the movement axis to capture richer spatiotemporal dynamics.

However, the current LD-MEA configuration constrains our ability to detect subtle spatial activity patterns. Future studies should leverage high-density arrays such as BioCAM DupleX [29], CMOS-MEA5000 [30], and MaxTwo [31], which, by virtue of their much larger electrode counts, enable pre-experimental screening of the most active or information-rich sites [10]. Our current centre-of-activity analysis shows no systematic drift toward the stimulated electrode. Implementing such high-density MEAs would refine the spatial partitioning step, potentially uncovering finer spatial dynamics and more comprehensively characterizing the full parameter landscape.

## 4.2 Braille Benchmark: Performance and Insights

In the Braille classification experiment using organoid outputs, we compare the classification performance of 8-dimensional data from a single organoid and 24-dimensional data from three organoids using an SVM classifier. Under the single-organoid condition,

the classification accuracy for 26 Braille classes is approximately 61%, and the response patterns are relatively consistent across different pressing depths. When using three organoids, the accuracy increases to 83%. From the perspective of the classifier, this is because increasing the data dimensionality tends to improve the linear separability of the data points [32]. From the internal perspective of the organoids, each organoid has different network connectivity, developmental stage, and response characteristics. By combining similar yet distinct responses from multiple organoids, a more comprehensive and richer feature representation can be formed, which helps the classifier define clearer decision boundaries. As shown in the noise robustness experiments, the three-organoid system shows a significantly smaller drop in accuracy after noise is added. This is because when a feature from one organoid is missing or unreliable, the other two organoids still provide stable and complementary information. Although this approach may seem redundant, it is commonly observed in biological systems, where degeneracy enables distinct neural circuits to substitute for one another [33], allowing predictive feedback loops in the visual cortex to fill in occluded information [34] and contextual cues in speech to reconstruct missing phonemes [35], thereby safeguarding perception against damage or noise.

When working with organoid outputs, which are relatively low-dimensional, traditional machine learning methods such as SVM and KNN are preferable due to their small number of parameters and simple model structure. Compared with neural networks, which are more complex, have larger parameter sizes, and require longer training times, these methods offer clear advantages in energy efficiency [36]. However, for tasks that involve more complex features, higher-dimensional data, or stricter accuracy requirements, and where energy consumption is less constrained, deep learning methods could be applied [37]. The present study relies on simple spike counts. Future work should evaluate temporal-pattern classifiers [11], population-vector readouts, graph-based methods, and other decoders, both in open and closed loop, to determine which metrics best capture the computation performed by the organoid.

### 4.3 Future Work

Neuromorphic tactile sensors and cerebral organoids both communicate through spikes. Although these spikes are converted into electrical pulses for stimulation, the encoding is designed to retain key spatiotemporal cues while reparameterizing sensor spikes into a stimulation space supported by the hardware interface. Future work should investigate how the organoid networks interpret and transform these encoded spike patterns to engage their internal neural circuitry, potentially uncovering deeper insights into the organoids' intrinsic neural processing capabilities [38]. Moreover, spike-derived stimulation could be further developed to facilitate clear channel-to-channel mapping, targeted neural activation, and biologically realistic starting points for adaptive, closed-loop bio-hybrid

systems that exhibit learning and plasticity [7, 13].

In addition to spike-driven encoding, the present encoder uses a fixed  $2 \times 4$  grid tuned to the Braille trajectory. Future work should explore varying the grid geometry, feature selection, and parameter quantisation to better understand how each factor influences classification accuracy, robustness, and energy efficiency. A wider task set including static indentation, texture tracking and edge orientation detection could test whether specific input statistics preferentially engage organoid circuitry or even induce experience-dependent plasticity [39].

Future studies should also implement closed-loop platforms, allowing organoid-generated spikes to influence subsequent inputs actively. Comparing open-loop and closed-loop conditions will reveal if feedback mechanisms enhance learning efficacy and induce significant changes in network dynamics. Such experiments can address the critical question of whether feedback is essential for organoid-based computation and adaptation [7]. Finally, a forward-looking goal is to route organoid output into peripheral or cortical tissue, creating a bidirectional bio-hybrid loop in which synthetic sensors drive the organoid and the organoid modulates living nerves. Such preparations could serve as testbeds for neuro-prosthetic [40] concepts before in-vivo implementation.

## **Conflict of Interest Statement**

The authors declare that the research was conducted in the absence of any commercial or financial relationships that could be construed as a potential conflict of interest.

## **Author Contributions**

TL: Conceptualization, Methodology, Investigation, Formal analysis, Writing – original draft; HP: Conceptualization, Methodology; BWC: Conceptualization, Supervision, Formal analysis, Writing – review & editing.

## **Funding**

This paper is funded by the China Scholarship Council.

## **Acknowledgments**

The authors thank FinalSpark for providing access to their Neuroplatform and neural organoid resources. We are grateful to the FinalSpark team for their technical support and valuable assistance during the experimental sessions.

## Supplemental Data

Not applicable.

## Data Availability Statement

All data needed to evaluate the conclusions in the paper are present in the paper.

## References

- [1] Filipp Akopyan, Jun Sawada, Andrew Cassidy, Rodrigo Alvarez-Icaza, John Arthur, Paul Merolla, Nabil Imam, Yutaka Nakamura, Pallab Datta, Gi-Joon Nam, et al. Truenorth: Design and tool flow of a 65 mw 1 million neuron programmable neurosynaptic chip. *IEEE transactions on computer-aided design of integrated circuits and systems*, 34(10):1537–1557, 2015.
- [2] Mike Davies, Narayan Srinivasa, Tsung-Han Lin, Gautham Chinya, Yongqiang Cao, Sri Harsha Choday, Georgios Dimou, Prasad Joshi, Nabil Imam, Shweta Jain, et al. Loihi: A neuromorphic manycore processor with on-chip learning. *Ieee Micro*, 38(1):82–99, 2018.
- [3] Adnan Mehonic and Anthony J Kenyon. Brain-inspired computing needs a master plan. *Nature*, 604(7905):255–260, 2022.
- [4] Jeewaka Perera, Sasitharan Balasubramaniam, Samitha Somathilaka, Qu Wen, Xu Li, Dharshana Kasthurirathna, Arman Roohi, and Tyler Nelson. Wet-neuromorphic computing: A new paradigm for biological artificial intelligence. *IEEE Intelligent Systems*, 2025.
- [5] Brett J Kagan, Forough Habibollahi, Brad Watmuff, Azin Azadi, Finn Doensen, Alon Loeffler, Seung Hoon Byun, Bram Servais, Candice Desouza, Kwaku Dad Abu-Bonsrah, et al. Harnessing intelligence from brain cells in vitro. *The Neuroscientist*, page 10738584251321438, 2025.
- [6] Hyogeun Shin, Sohyeon Jeong, Ju-Hyun Lee, Woong Sun, Nakwon Choi, and Il-Joo Cho. 3d high-density microelectrode array with optical stimulation and drug delivery for investigating neural circuit dynamics. *Nature communications*, 12(1):492, 2021.
- [7] Forough Habibollahi, Brett J Kagan, Anthony N Burkitt, and Chris French. Critical dynamics arise during structured information presentation within embodied in vitro neuronal networks. *Nature Communications*, 14(1):5287, 2023.

- [8] Tal Sharf, Tjitse Van Der Molen, Stella MK Glasauer, Elmer Guzman, Alessio P Buccino, Gabriel Luna, Zhuowei Cheng, Morgane Audouard, Kamalini G Ranasinghe, Kiwamu Kudo, et al. Functional neuronal circuitry and oscillatory dynamics in human brain organoids. *Nature communications*, 13(1):4403, 2022.
- [9] Felix Franke, Michele Fiscella, Maksim Sevelev, Botond Roska, Andreas Hierlemann, and Rava Azeredo da Silveira. Structures of neural correlation and how they favor coding. *Neuron*, 89(2):409–422, 2016.
- [10] Hongwei Cai, Zheng Ao, Chunhui Tian, Zhuhao Wu, Hongcheng Liu, Jason Tchieu, Mingxia Gu, Ken Mackie, and Feng Guo. Brain organoid reservoir computing for artificial intelligence. *Nature Electronics*, 6(12):1032–1039, 2023.
- [11] Joël Küchler, Katarina Vulić, Haotian Yao, Christian Valmaggia, Stephan J Ihle, Sean Weaver, and János Vörös. Engineered biological neuronal networks as basic logic operators. *Frontiers in Computational Neuroscience*, 19:1559936, 2025.
- [12] Richard George, Michela Chiappalone, Michele Giugliano, Timothée Levi, Stefano Vassanelli, Johannes Partzsch, and Christian Mayr. Plasticity and adaptation in neuromorphic biohybrid systems. *Science*, 23(10), 2020.
- [13] Craig Ades, Moaed A Abd, Douglas T Hutchinson, Emmanuelle Tognoli, E Du, Jianning Wei, and Erik D Engeberg. Biohybrid robotic hand to investigate tactile encoding and sensorimotor integration. *Biomimetics*, 9(2):78, 2024.
- [14] Brett J Kagan, Andy C Kitchen, Nhi T Tran, Forough Habibollahi, Moein Khajehnejad, Bradyn J Parker, Anjali Bhat, Ben Rollo, Adeel Razi, and Karl J Friston. In vitro neurons learn and exhibit sentience when embodied in a simulated game-world. *Neuron*, 110(23):3952–3969, 2022.
- [15] Xingyuan Xu, Zhengjie Liu, Jing Liu, Chuanjie Yao, Xi Chen, Xinshuo Huang, Shuang Huang, Peng Shi, Mingqiang Li, Li Wang, et al. Multi-sized microelectrode array coupled with micro-electroporation for effective recording of intracellular action potential. *Microsystems & Nanoengineering*, 11(1):1–18, 2025.
- [16] Fred D Jordan, Martin Kutter, Jean-Marc Comby, Flora Brozzi, and Ewelina Kurtys. Open and remotely accessible neuroplatform for research in wetware computing. *Frontiers in Artificial Intelligence*, 7:1376042, 2024.
- [17] Matteo Cartiglia, Filippo Costa, Shyam Narayanan, Cat-Vu H Bui, Hasan Ulasan, Nicoletta Risi, Germain Haessig, Andreas Hierlemann, Fernando Cardes, and Giacomo Indiveri. A 4096 channel event-based multielectrode array with asynchronous outputs compatible with neuromorphic processors. *Nature Communications*, 15(1):7163, 2024.

- [18] Corinna Cortes and Vladimir Vapnik. Support-vector networks. *Machine learning*, 20:273–297, 1995.
- [19] Subashika Govindan, Laura Batti, Samira F Osterop, Luc Stoppini, and Adrien Roux. Mass generation, neuron labeling, and 3d imaging of minibrains. *Frontiers in bioengineering and biotechnology*, 8:582650, 2021.
- [20] Stuart F Cogan. Neural stimulation and recording electrodes. *Annu. Rev. Biomed. Eng.*, 10(1):275–309, 2008.
- [21] Daniel A Wagenaar, Jerome Pine, and Steve M Potter. Effective parameters for stimulation of dissociated cultures using multi-electrode arrays. *Journal of neuroscience methods*, 138(1-2):27–37, 2004.
- [22] Niklas Funk, Erik Helmut, Georgia Chalvatzaki, Roberto Calandra, and Jan Peters. Evetac: An event-based optical tactile sensor for robotic manipulation. *IEEE Transactions on Robotics*, 2024.
- [23] Shenzhen Yuejiang Technology Co., Ltd. *Dobot MG400 Desktop-Grade 4-Axis Robotic Arm User Guide*, 2020.
- [24] Kwabena A Boahen. Point-to-point connectivity between neuromorphic chips using address events. *IEEE Transactions on Circuits and Systems II: Analog and Digital Signal Processing*, 47(5):416–434, 2002.
- [25] Thomas Cover and Peter Hart. Nearest neighbor pattern classification. *IEEE transactions on information theory*, 13(1):21–27, 1967.
- [26] Leo Breiman. Random forests. *Machine learning*, 45:5–32, 2001.
- [27] Vincent Chan, Shih-Chii Liu, and Andr van Schaik. Aer ear: A matched silicon cochlea pair with address event representation interface. *IEEE Transactions on Circuits and Systems I: Regular Papers*, 54(1):48–59, 2007.
- [28] Thomas L Li, Yuxin Liu, Csaba Forro, Xiao Yang, Levent Beker, Zhenan Bao, Bianxiao Cui, and Sergiu P Paşca. Stretchable mesh microelectronics for the biointegration and stimulation of human neural organoids. *Biomaterials*, 290:121825, 2022.
- [29] 3 Brain. Biocam duplex: Bidirectional hd-mea for 2d and 3d systems. Available at: <https://www.3brain.com/products/single-well/biocam-duplex>, 2019.
- [30] Multi Channel Systems. Cmos-mea5000 system. Available at: <https://www.multichannelsystems.com/products/cmos-mea5000-system>, 2015.

- [31] MaxWell Biosystems. Maxtwo multiwell high-density microelectrode array system. Available at: <https://www.mxwbio.com/products/maxtwo-multiwell-microelectrode-array/>, 2019.
- [32] Thomas M Cover. Geometrical and statistical properties of systems of linear inequalities with applications in pattern recognition. *IEEE transactions on electronic computers*, (3):326–334, 2006.
- [33] Karl J Friston and Cathy J Price. Degeneracy and redundancy in cognitive anatomy. *Trends in cognitive sciences*, 7(4):151–152, 2003.
- [34] Rajesh PN Rao and Dana H Ballard. Predictive coding in the visual cortex: a functional interpretation of some extra-classical receptive-field effects. *Nature neuroscience*, 2(1):79–87, 1999.
- [35] Richard M Warren. Perceptual restoration of missing speech sounds. *Science*, 167(3917):392–393, 1970.
- [36] Emma Strubell, Ananya Ganesh, and Andrew McCallum. Energy and policy considerations for modern deep learning research. In *Proceedings of the AAAI conference on artificial intelligence*, volume 34, pages 13693–13696, 2020.
- [37] Nur Ahmadi, Timothy G Constandinou, and Christos-Savvas Bouganis. Robust and accurate decoding of hand kinematics from entire spiking activity using deep learning. *Journal of Neural Engineering*, 18(2):026011, 2021.
- [38] Tatsuya Osaki, Tomoya Duenki, Siu Yu A Chow, Yasuhiro Ikegami, Romain Beaubois, Timothée Levi, Nao Nakagawa-Tamagawa, Yoji Hirano, and Yoshiho Ikeuchi. Complex activity and short-term plasticity of human cerebral organoids reciprocally connected with axons. *Nature communications*, 15(1):2945, 2024.
- [39] Ash Robbins, Hunter E Schweiger, Sebastian Hernandez, Alex Spaeth, Kateryna Voitiuk, David F Parks, Tjitse Van der Molen, Jinghui Geng, Tal Sharf, Mohammed A Mostajo-Radji, et al. Goal-directed learning in cortical organoids. *bioRxiv*, pages 2024–12, 2024.
- [40] Calogero Maria Oddo, Stanisa Raspopovic, Fiorenzo Artoni, Alberto Mazzoni, Giacomo Spigler, Francesco Petrini, Federica Giambattistelli, Fabrizio Vecchio, Francesca Miraglia, Loredana Zollo, et al. Intranural stimulation elicits discrimination of textural features by artificial fingertip in intact and amputee humans. *elife*, 5:e09148, 2016.